Title
MAGNETIC FIELD CALCULATIONS FOR THE 184-INCH SYNCHROCYCLOTRON

Authors
Paul, A.C.
Colonias, J.S.
Paul, A.C.
et al.

Publication Date
1970-02-01

UCRL-18882 c.2 rev.
UC-28
Particle Accelerators
and High-Voltage Mach.
TID-4500 (55th Ed.)

MAGNETIC FIELD CALCULATIONS FOR THE 184-INCH SYNCHROCYCLOTRON

A. C. Paul and J. S. Colonias

February 1970

AEC Contract No. W-7405-eng-48

LAWRENCE RADIATION LABORATORY
UNIVERSITY of CALIFORNIA BERKELEY

UCRL-18882 c.2 rev.

DISCLAIMER

MAGNETIC FIELD CALCULATIONS FOR THE 184-INCH SYNCHROCYCLOTRON

A. C. Paul and J. S. Colonias
Lawrence Radiation Laboratory
University of California
Berkeley, California 94720

February 1970

I. ABSTRACT

This paper describes our experiences with the use of a computer program to calculate the magnetic field change produced by a change in the coil excitation of the Berkeley 184-inch synchrocyclotron.

One of the interesting aspects of these calculations is the simulation of the magnet with a cylindrical pole face and a rectangular return yoke. The raw computed magnetic field compares to the azimuthally averaged measured field at the same excitation to within 1%.

A subtraction technique is used to cancel integration and systematic model errors and yields a calculated magnetic field that compares to within 0.1% with the measured fields at different excitations.

The calculations include the effects of the plate construction (stacking factor) of the magnet and assume median-plane symmetry, but do not include the small effects produced by the main-coil current symmetry shunts and nonuniform current distribution, although these could have been included.

II. INTRODUCTION

The field calculations reported herein were undertaken in order to determine if the change in the radial magnetic field profile of the 184-inch cyclotron produced by a corresponding change in the coil excitation could be calculated by computer modeling.

Two such models were constructed, one representing the 184-inch cyclotron magnet at the time of the 1957 field measurements and the other representing it at the time of the 1968 field measurements.

We find that the computed change in field produced by a change in coil excitation is in agreement with that measured for each model, to within 0.1%.

III. MAGNETIC FIELD MEASUREMENTS

The last complete magnetic field measurements were made during the conversion of the 184-inch cyclotron from 340 to 740 MeV in 1957. These measurements included a standard field with main-coil excitation of 1530 A, auxiliary coil excitation of 2660 A also at a main-coil setting of 1524 A for auxiliary coil currents of 2441, 2662, and 2743 A. We did not know at the time that the bottom pie of the lower main coil was intermittently shorting. In 1958 this pie was permanently disconnected and the excitations of the coils were adjusted for best operation. In 1962 the current-monitoring shunts were repaired without recalibration, so that when the calculations reported here were begun the magnetic field

was believed to be 200 to 300 G higher than the 1957 measurements indicated.

In February 1968 we measured the field along the azimuth of the main probe (105 deg) at a standard auxiliary coil current of 2678 A for three different main-coil currents of 1500, 1562, and 1620 A. These currents are based on a new (1968) shunt calibration. The field measurements undertaken at 105 deg provide the experimental data necessary to determine what effect a change in the main-coil exitation produces on the field, but are not indicative of the actual radial field. This is because at this azimuth the probe passes sufficiently close to the regenerator and regenerator compensation shims to see strong local field perturbations. The present measured field is approximately 100 G higher than the 1957 measurements.

IV. THE COMPUTER CALCULATIONS

The calculations were performed by simulating the cyclotron magnet shown in Fig. 1 by a computer program called TRIM.[1] This program solves the two-dimensional magnetostatic problem by iterative overrelaxation of the finite-difference equation approximating the differential equation for the magnetic vector potential, $\vec{A}$,

$$\vec{\nabla} \cdot \left[\frac{1}{\mu r} \vec{\nabla} (r\vec{A}) \right] = - 4\pi \vec{J}, \qquad (1)$$

where μ is the permeability of the material and J is the current density. The computational model in TRIM consists of an irregular triangular mesh of approximately 4000 points.[2] The magnet geometry is outlined in Fig. 2 and shows the computer-generated mesh of the 184-inch cyclotron magnet. Azimuthal and median-plane symmetry is required, so the magnet return yoke thickness was adjusted for constant area in cylindrical geometry, although the actual yoke is rectangular. The exact magnet gap and the curved approximation used by TRIM are shown in Fig. 3. The gap has been corrected for radial distortions produced by magnetic loading,[3] and is given in Table I. The average gap reduction produced by vacuum loading is 0.018 inch.[3]

V. FIELD CALCULATIONS

Figure 4 shows the pie configuration of the coils. The bottom pie of the lower main coil (B1) was intermittently shorting at the time of the 1957 field measurements. This short was not discovered until a year after the measurements were completed. We have therefore calculated the magnetic field at each excitation used during the 1957 measurements with the B1 pie both in the circuit and out of the circuit.

Figure 5 shows a computer plot of the magnetic field flux lines generated by TRIM. These lines of flux should be interpreted as lines of constant $r\vec{A}$.

Figure 6 shows a computer plot of the median-plane magnetic field calculated by TRIM at the coil excitations at the standard 1957 measurements, along with the azimuthally averaged measured field at the same excitation.

Figures 7, 8, and 9 show the calculated fields (TRIM-10, TRIM-11, TRIM-12, TRIM-19, TRIM-20, and TRIM-25) and the measured fields at 162 deg azimuth. Comparing the calculated curves with those of Fig. 6, we see that apparently the B1 pie was not shorted at the auxiliary coil current of 2441 A, but was shorted at 2662 and 2743 A.

TRIM converged after 700 iterations and required 40 minutes of computer time on the CDC-6600. These calculations were carried out for the coil excitations given in Table II. The reciprocal of the iron permeability used in the calculations as a function of the square of the magnetic field is given in

Table III.

The difference between the calculated field at various excitations and the calculated field at the standard excitation of the 1957 measurements (TRIM-8) should give the field change produced by the change in coil excitation, provided the integration errors are independent of excitation. Figure 10 shows the "smoothed" calculated median plane radial field profiles obtained by adding the difference between the calculated profile and TRIM-8 to the standard 1957 measured field. The calculated change in field produced by alteration of coil excitation and the measured change in field are in excellent agreement.

Figure 11 shows the 1968 measured magnetic fields obtained along the 105-deg probe line at three different main coil excitations and the calculated field profiles at the corresponding coil excitation. The bumps in the radial measured field reflect the close proximity of the magnetic regenerator centered at 116 deg. No attempt has been made to average the field azimuthally. However, the calculated change in field produced by alteration of coil excitation and the measured change in field are in excellent agreement. Figure 12 shows the "smoothed" field.

Figures 13 and 14 show the effect of the alteration of excitation on the radial field falloff. Here, all smoothed calculated fields have been normalized to 23 075 G at 15 in. radius. The increase in field falloff at higher excitations is obvious, and results from increased saturation near the pole edge.

VI. 1968 MEASURED FIELD

Figure 15 shows the 1957 and 1968 measured standard field and the computer-calculated field for present (1969) cyclotron excitations before correction for stacking factor or size of universe (see Section VII). The 1968 data (extending from 50 to 94 in. at 105 deg have been smoothed to eliminate the effect of the regenerator perturbations by subtraction of the 1957 data at the same azimuth and adding the difference to the 1957 standard field. The field between 2 and 50 in. is a smooth joint to the 1957 field scaled to match the 1968 data at 50 in.

The 1968 field measurements show that the magnetic field under present operating conditions is approximately 100 G higher than in 1957. The parameters defined by the new magnetic field and radius are summarized in Table IV. Here the proton energy E (MeV) is found from the magnetic rigidity B (gauss), R (inches), and the rest energy $E_0 = 938.213$ MeV:

$$E = E_0 \sqrt{1 + \left(\frac{BR}{1.232103 \times 10^6} \right)^2} .$$

Gamma is defined as $\gamma \equiv E/E_0$. The rotational frequency F (in hertz) of protons in this magnetic field B (in gauss) is expressed by $F \equiv 1526.73\ B/\gamma$. The vertical and radial betatron oscillation frequencies in terms of the rotational frequencies are given by $\nu_z \equiv n^{1/2}$, $\nu_r \equiv (1-n)^{1/2}$, where n is the usual field index determined by $-(dB/dR)(R/B)$.

Orbit calculations using the magnetic field, including the measured regenerator perturbations, show that the radial betatron phase space vanishes at 82.15 in., i.e., 747 MeV. Since the time of the field measurements the regenerator was moved outward 0.25 in., which should increase the beam energy by approximately 3 MeV to 750 MeV. This is then the maximum energy obtainable in the external beam for present operating conditions. The external beam energy at the peak in the particle spectrum is less than the maximum energy, since the available radial betatron phase space becomes smaller as the energy increases (smaller radial betatron amplitude). We find that the peak in the energy spectrum

for the measured internal radial betatron phase-space distribution[4] occurs about 4 MeV below the maximum energy. The energy at the peak in the particle spectrum for the external beam should then be 746 MeV.

The energy of the external physics cave proton beam has recently been measured[5] by determining its range in copper. Analysis of the data was undertaken with the computer code BRAGG,[6] based on the range energy calculations by Steward and Wallace.[7] The energy for the mean range was found to be 746 MeV. No corrections were made for the 6 in. of air preceding and following the copper or the aluminum exit window. Earlier, Freisen and Barkas[8] measured the beam energy and found it to be 747 MeV according to the range energy relations of Sternheimer. The calculated energy compares favorably with the measured energy.

VII. FURTHER COMPUTER MODEL IMPROVEMENTS

The finite mesh size (4000 points) that TRIM is capable of handling necessitated the approximation of the 184-inch cyclotron magnet with insufficient air border, which forces the fringing field through the magnetic core, producing a smaller field in the pole. The reason for this is the basic assumption in program TRIM, which does not allow any flux to escape the boundary of the "universe" in which the magnet geometry is described. In other words, the vector potential $\vec{A}$ is zero at a nonreflecting boundary and it is not relaxed. This by no means restricts the program, since the variable-mesh feature of TRIM allows an expansion of the mesh to any arbitrary physical dimensions, as can be seen in Fig. 16.

Also, the steel in the yoke of the magnet is not solid, but consists of welded plates each 1.5 in. thick. Therefore the lamination stacking factor produced by the air and oxide surfaces reduces the total iron by about 2%. These effects were included in the modified computer model, and the results are shown in Figs. 17, 18, and 19. Here, 1000 points were allocated to describe the magnet geometry with uniform gap, and the remaining 3000 points were used for an air border (Fig. 16). The dimensions of the "universe" were enlarged to 1000×1000 in. from the magnet universe of 180×312 in. The resulting flux distribution is shown in Fig. 17.

Figures 18a and b show the same geometry with the "universe" reduced to 365×1000 in.

The results of using these models with stacking-factor variations are given in Table V. It will be noticed that the effect of reducing the stacking factor is to reduce the field, whereas the effect of increasing the size of the universe is to increase the field. Figure 19 shows the change in field, ΔB, vs radius, R, for the cases listed in Table V referenced to the standard computer model (stacking factor 1., universe of 180×312 in.), described in Section V. The effect of a universe change beyond 1000×1000 in. is small, so we do not consider larger universes. The 184-inch magnet should have a stacking factor of approximately 0.96. These corrections increase the calculated field by approximately 170 G, raising the calculated field at 70 in. from 22 400 to 22 570 G. The measured field at 70 in. is 22 514 G.

CONCLUSIONS

This paper shows that the field of a large synchrocyclotron can be calculated from a computer model to within 1%, and changes in the field produced by excitation changes can be calculated to within 0.1%, provided correction is made for the stacking factor and air boundary around the magnetic iron. (We are indebted to C. Dols for pointing this out.) The importance of this air boundary was not

sufficiently appreciated by the authors when this work was undertaken, and is of considerable importance in a highly saturated magnet such as the 184-inch cyclotron.

ACKNOWLEDGMENTS

The authors express their appreciation for several enlightening discussions of the 1957 field measurements with Joseph H. Dorst and Chuck Dols. Peter Watson made the 1968 field measurements, and Howard Heath performed the 1968 shunt calibration. The assistance of James L. MacMullen and Leal L. Kanstein in performing the range measurement is also acknowledged.

REFERENCES

1. John S. Colonias, TRIM: A Magnetostatic Computer Program for the CDC 6600, Lawrence Radiation Laboratory Report UCRL-18439, Aug. 1968.
2. A. M. Winslow, Magnetic Field Calculations in an Irregular Triangular Mesh, ibid. p. 170.
3. Lawrence Radiation Laboratory Engineering Note 4121-12-M30 and M31 (1956).
4. A. C. Paul, Study of the Regenerative Extractor of the Berkeley 184-Inch Synchrocyclotron UCRL-18211, April 1968.
5. A. C. Paul, unpublished data.
6. G. M. Litton, Program BRAGG for Calculating Bragg Curves and Flux Distributions, UCRL-17391 Feb. 1967.
7. P. G. Steward and R. W. Wallace, Calculation of Stopping Power and Range Energy Values for Any Heavy Ion in Nongaseous Media, UCRL-17314, Dec. 1966.
8. S. Von Friesen and W. H. Barkas, Structure of External Beam of the 184-Inch Cyclotron, UCID-613 Jan. 1969.

Table I. 184-Inch cyclotron gap vs. radius.

Shim Number	Magnet gap: Inner radius (in.)	Magnet gap: Outer radius (in.)	Magnet gap: Half gap (in.)
1	0	6	7.569
2	6	9	7.603
3	9	12	7.625
4	12	16.2	7.633
5	16.2	33	7.693
6	33	39.5	7.684
7	39.5	44	7.654
8	44	47.5	7.611
9	47.5	50.0	7.576
10	50	52.5	7.540
11	52.5	54.5	7.498
12	54.5	57	7.459
13	57	60.11	7.385
14	60.11	63.68	7.308
15	63.68	68.14	7.123
16	68.14	72.21	6.951
17	72.21	75.79	6.697
18	75.79	78.34	6.448
19	78.34	80.12	6.294
20	80.12	81.12	6.315
21	81.12	83.125	5.905
--	83.125	91.0	5.593

Table II. Coil excitations used in calculations.

Trim run	Measured field	Fig.	Turns per aux. coil	Aux. coil (mV)	Aux. coil current (A)	Av. turns per main coil	Main coil B1 pie	Main coils (mV)	Main coil current (A)
8 standard	6-21-67 standard	6	212.5	469.8	2660	1307	in	486.63	1530/2
10	6-21-67 run 467, 162 deg, aux. coil	7	212.5	430.52	2441	1235	out	486.40	1524/2
20	2500 A nominal	7	212.5	430.52	2441	1307	in	486.40	1524/2
11	6-21-57 run 463, 162 deg, aux. coil	8	212.5	469.46	2662	1235	out	486.40	1524/2
25	2700 A nominal	8	212.5	469.46	2662	1307	in	486.40	1524/2
12	6-21-57 run 474, 162 deg, aux. coil	9	212.5	483.85	2743	1235	out	486.40	1524/2
19	2800 A nominal	9	212.5	483.85	2743	1307	in	486.40	1524/2
22 present operating conditions	2-29-68 field meas. at 105 deg, aux. coil constant at 3 main coil field settings	11	212.5	492.73	2678	1239	out	520.40	1562/2
23		11	212.5	492.73	2678	1239	out	500.00	1501/2
24		11	212.5	492.73	2678	1239	out	540.00	1620/2

Table III. Permeability table used in calculating μ vs B^2.

B^2	$1/\mu$
0.	2.250000×10^{-4}
1.440000×10^{8}	3.080000×10^{-4}
1.960000×10^{8}	4.500000×10^{-4}
2.250000×10^{8}	6.670000×10^{-4}
2.402500×10^{8}	9.350000×10^{-4}
2.560000×10^{8}	1.410000×10^{-3}
2.722500×10^{8}	2.180000×10^{-3}
2.890000×10^{8}	3.240000×10^{-3}
3.062500×10^{8}	4.340000×10^{-3}
3.240000×10^{8}	5.670000×10^{-3}
3.422500×10^{8}	7.190000×10^{-3}
3.610000×10^{8}	9.000000×10^{-3}
3.802500×10^{8}	1.110000×10^{-2}
4.000000×10^{8}	1.330000×10^{-2}
4.202500×10^{8}	1.640000×10^{-2}
4.410000×10^{8}	2.020000×10^{-2}
4.515600×10^{8}	2.260000×10^{-2}
4.622500×10^{8}	2.560000×10^{-2}
4.730620×10^{8}	3.030000×10^{-2}
4.840000×10^{8}	3.770000×10^{-2}
5.062500×10^{8}	5.560000×10^{-2}
5.197030×10^{8}	6.666700×10^{-2}
5.321600×10^{8}	7.692300×10^{-2}
5.495740×10^{8}	9.090900×10^{-2}
5.757890×10^{8}	1.111110×10^{-1}
6.202590×10^{8}	1.428700×10^{-1}
7.131570×10^{8}	2.000000×10^{-1}
9.968920×10^{8}	3.333330×10^{-1}
1.473796×10^{10}	8.237230×10^{-1}
1.000000×10^{20}	1.000000

Table IV. Calculated field properties for present field.

R (in.)	B (G)	n	γ	E (MeV)	F (MHz)	ν_z	ν_r
10	53249	.00738	1.0176	16.6	34.88	.0859	.9963
11	53232	.00801	1.0213	20.0	34.73	.0895	.9960
12	53215	.00909	1.0252	23.7	34.57	.0954	.9954
13	53197	.01012	1.0295	27.7	34.40	.1006	.9949
14	53179	.01120	1.0341	32.0	34.22	.1058	.9944
15	53160	.01240	1.0390	36.6	34.03	.1114	.9938
16	53141	.01333	1.0442	41.4	33.83	.1155	.9933
17	53122	.01334	1.0497	46.6	33.63	.1155	.9933
18	53104	.01288	1.0554	52.0	33.42	.1135	.9935
19	53088	.01244	1.0615	57.7	33.21	.1115	.9938
20	53074	.01151	1.0678	63.7	32.99	.1073	.9942
21	53061	.01193	1.0745	69.9	32.77	.1092	.9940
22	53048	.01199	1.0814	76.3	32.54	.1095	.9940
23	53036	.01192	1.0885	83.1	32.31	.1092	.9940
24	53024	.01244	1.0960	90.0	32.07	.1116	.9938
25	53012	.01364	1.1036	97.2	31.83	.1169	.9931
26	52999	.01475	1.1116	104.7	31.59	.1215	.9926
27	52986	.01588	1.1197	112.3	31.34	.1260	.9920
28	52972	.01733	1.1281	120.2	31.09	.1316	.9913
29	52958	.01755	1.1367	128.2	30.84	.1325	.9912
30	52944	.01899	1.1455	136.5	30.58	.1378	.9905
31	52929	.02072	1.1545	144.9	30.32	.1439	.9896
32	52914	.02024	1.1637	153.6	30.06	.1423	.9898
33	52900	.02026	1.1731	162.4	29.80	.1423	.9898
34	52886	.02013	1.1827	171.4	29.54	.1419	.9899
35	52873	.01997	1.1925	180.6	29.28	.1413	.9900
36	52860	.01976	1.2025	190.0	29.02	.1406	.9901
37	52848	.01950	1.2127	199.6	28.76	.1397	.9902
38	52835	.01920	1.2231	209.3	28.50	.1386	.9904
39	52824	.01891	1.2337	219.2	28.25	.1375	.9905
40	52813	.01830	1.2444	229.3	27.99	.1353	.9908
41	52803	.01870	1.2553	239.5	27.73	.1368	.9906
42	52792	.02065	1.2664	249.9	27.48	.1437	.9896
43	52781	.02077	1.2775	260.4	27.22	.1441	.9896
44	52770	.02133	1.2889	271.0	26.97	.1461	.9893
45	52759	.02189	1.3004	281.8	26.72	.1480	.9890
46	52748	.02206	1.3120	292.7	26.47	.1485	.9889
47	52737	.02386	1.3237	303.7	26.22	.1545	.9880
48	52725	.02572	1.3356	314.9	25.98	.1604	.9871
49	52713	.02592	1.3476	326.1	25.73	.1610	.9870
50	52701	.02647	1.3597	337.4	25.49	.1627	.9867
51	52689	.02737	1.3719	348.9	25.25	.1654	.9862
52	52677	.02648	1.3842	360.4	25.01	.1627	.9867
53	52666	.02543	1.3966	372.1	24.78	.1595	.9872
54	52655	.02671	1.4092	383.9	24.54	.1634	.9866
55	52644	.02558	1.4219	395.8	24.31	.1599	.9871
56	52634	.02459	1.4347	407.8	24.09	.1568	.9876
57	52624	.02498	1.4476	419.9	23.86	.1580	.9874
58	52614	.02715	1.4605	432.1	23.64	.1648	.9863
59	52603	.02874	1.4736	444.3	23.42	.1695	.9855
60	52593	.02292	1.4868	456.7	23.20	.1514	.9885
61	52586	.01534	1.5001	469.2	22.99	.1238	.9923
62	52581	.01308	1.5136	481.9	22.78	.1144	.9934
63	52576	.01487	1.5272	494.7	22.57	.1219	.9925
64	52570	.02007	1.5409	507.5	22.36	.1417	.9899
65	52561	.02458	1.5546	520.3	22.16	.1568	.9876
66	52552	.02920	1.5683	533.1	21.96	.1709	.9853
67	52541	.03504	1.5819	546.0	21.75	.1872	.9823
68	52529	.03651	1.5956	558.8	21.56	.1911	.9816
69	52517	.03707	1.6094	571.7	21.36	.1925	.9813
70	52505	.03665	1.6232	584.7	21.17	.1914	.9815
71	52494	.03168	1.6371	597.8	20.98	.1780	.9840
72	52485	.02656	1.6512	611.0	20.79	.1630	.9866
73	52477	.02582	1.6654	624.3	20.61	.1607	.9870
74	52469	.02663	1.6796	637.6	20.42	.1632	.9866
75	52461	.02625	1.6939	651.0	20.24	.1620	.9868
76	52453	.02933	1.7083	664.5	20.07	.1713	.9852
77	52444	.02968	1.7226	678.0	19.89	.1723	.9850
78	52436	.02757	1.7371	691.8	19.72	.1661	.9861
79	52428	.02783	1.7516	705.1	19.55	.1668	.9860
80	52420	.03117	1.7661	718.8	19.38	.1765	.9843
81	52408	.06349	1.7805	732.3	19.21	.2520	.9677
82	52380	.15221	1.7940	744.9	19.05	.3901	.9208
83	52318	.32478	1.8056	755.9	18.87	.5699	.8217
84	52197	.59510	1.8139	763.6	18.68	.7714	.6363
85	51996	.95534	1.8173	766.8	18.48	.9774	.2113
86	51697	1.40081					
87	51287	1.91367					
88	50761	2.47208					
89	50117	3.13890					
90	49336	3.97497					
91	48414	4.84768					
92	47391	5.59515					
93	46316	6.18324					
94	45236	6.58797					
95	44188	6.87672					
96	43181	7.19073					
97	42214	7.51374					
98	41291	7.79458					
99	40418	8.06283					
100	9595	8.30213					

Table V. Median plane magnetic field as function of radius for various stacking factors, pole surface contours, and universe sizes.

Top Boundary (in.)	180	180	180	200	365	1000	1000	180
Side Boundary (in.)	312	312	312	352	1000	1000	1000	312
Stacking factor	1.0	1.0	0.98	1.0	1.0	1.0	0.98	0.94
Gap (pole)	Tapered	Flat	Flat	Tapered	Flat	Flat	Flat	Flat
Total ampere turns			1537082.6			1537082.6	1537082.6	
Radius (in.)								
4.1364	23197	23089	22921	23363	23586	23626	23458	22578
8.2727	23206	23465	23294	23371	23967	24007	23835	22945
12.409	23141	23559	23386	23304	24060	24099	23927	23036
16.545	23057	23573	23401	23221	24074	24114	23941	23050
20.681	22988	23572	23399	23152	24072	24111	23938	23048
24.818	22932	23551	23378	23095	24050	24089	23918	23028
28.954	22868	23519	23347	23034	24018	24057	23885	22997
33.09	22799	23477	23305	22963	23975	24014	23843	22957
37.22	22726	23425	23254	22890	23923	23962	23792	22907
41.36	22659	23363	23192	22824	23860	23899	23729	22847
45.50	22601	23288	23118	22764	23784	23823	23654	22775
49.63	22546	23199	23030	22709	23694	23733	23564	22689
53.77	22494	23093	22924	22655	23585	23624	23457	22586
57.909	22440	22965	22797	22599	23454	23492	23326	22460
62.04	22391	22808	22641	22548	23293	23331	23166	22308
66.18	22365	22613	22448	22520	23092	23130	22967	22117
70.318	22345	22364	22201	22498	22836	22873	22711	21874
74.454	22331	22029	21869	22482	22489	22526	22366	21545
78.59	22318	21539	21381	22467	21984	22019	21862	21063
82.727	22140	20719	20565	22284	21144	21177	21025	20257
86.863	20866	19047	18906	21006	19450	19482	19343	18621
91.000	17116	15629	15516	17256	16018	16049	15937	15287
98.50	8976	8559	8505	9149	8945	8977	8924	8395
106.000	4493	4594	4565	4716	4985	5017	4988	4506

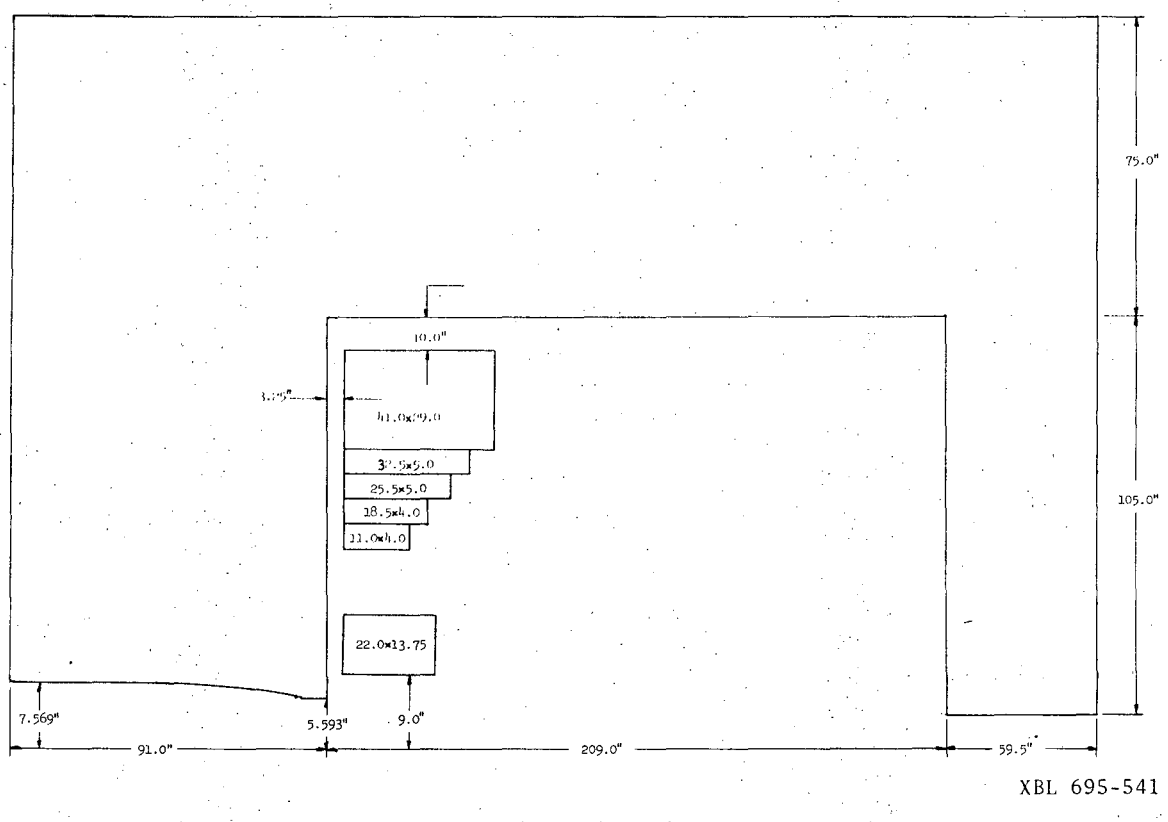

XBL 695-541

Fig. 1. The 184-inch cyclotron magnet.

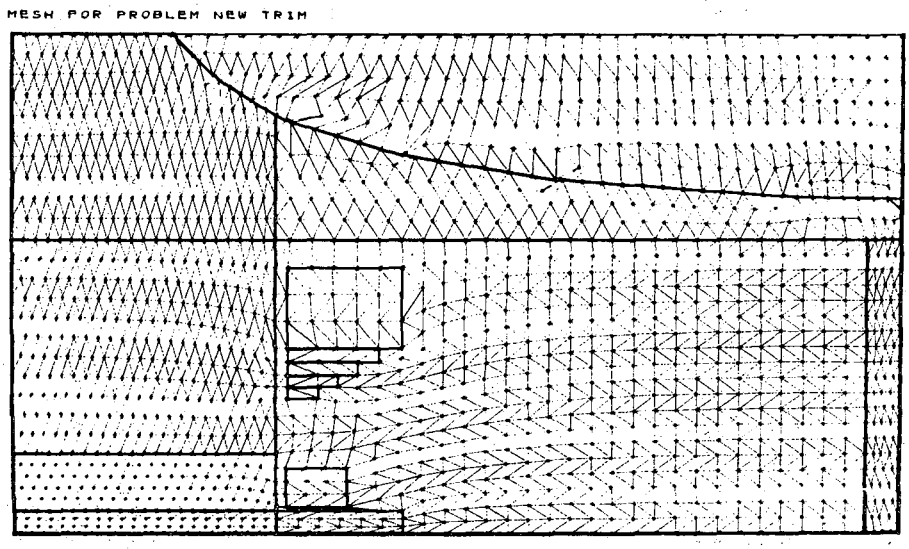

XBL 706-1075

Fig. 2. Triangular mesh generated by TRIM, no air boundary.

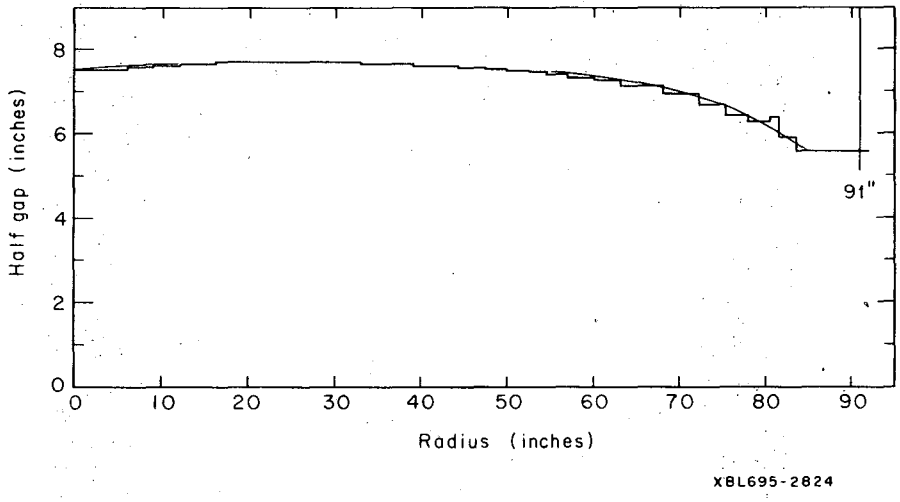

XBL695-2824

Fig. 3. 184-Inch cyclotron magnet gap and the smooth curved approximation used by TRIM.

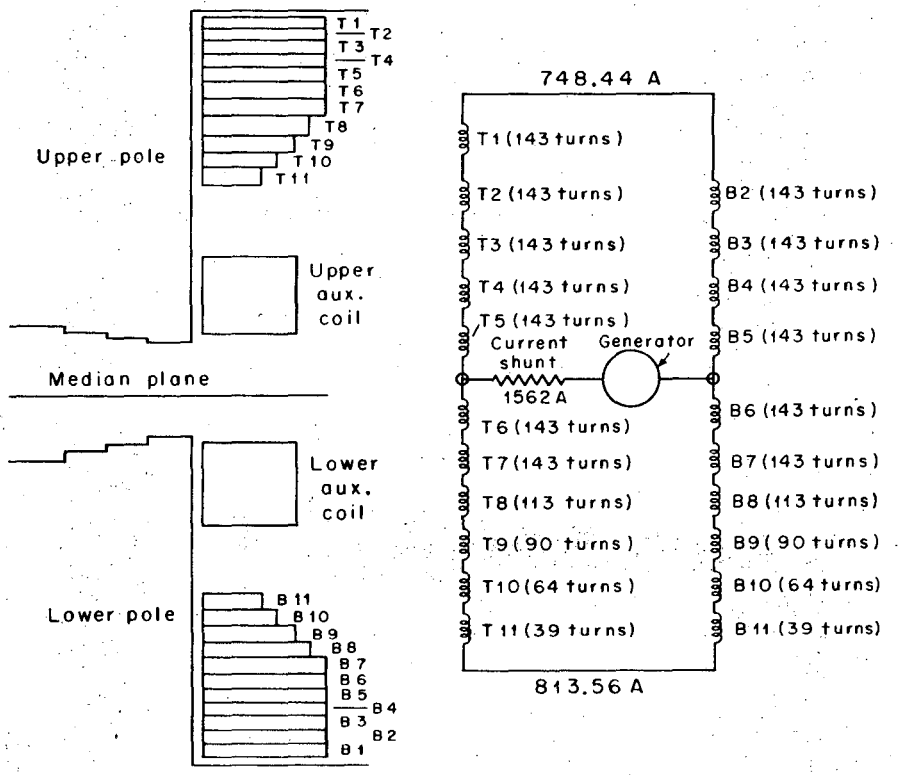

XBL695-2825

Fig. 4. Magnet coil and current distribution.

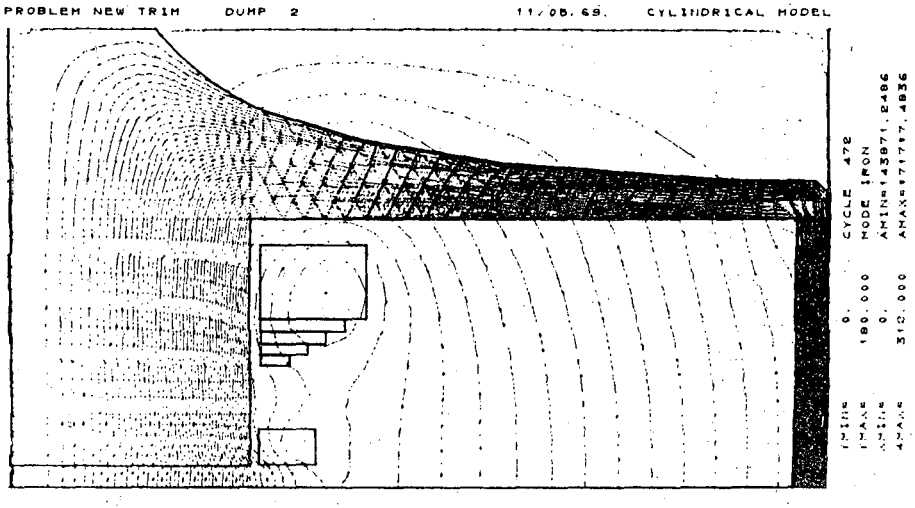

XBL 706-1076

Fig. 5. Magnet outline and computed magnetic flux, no air boundary.

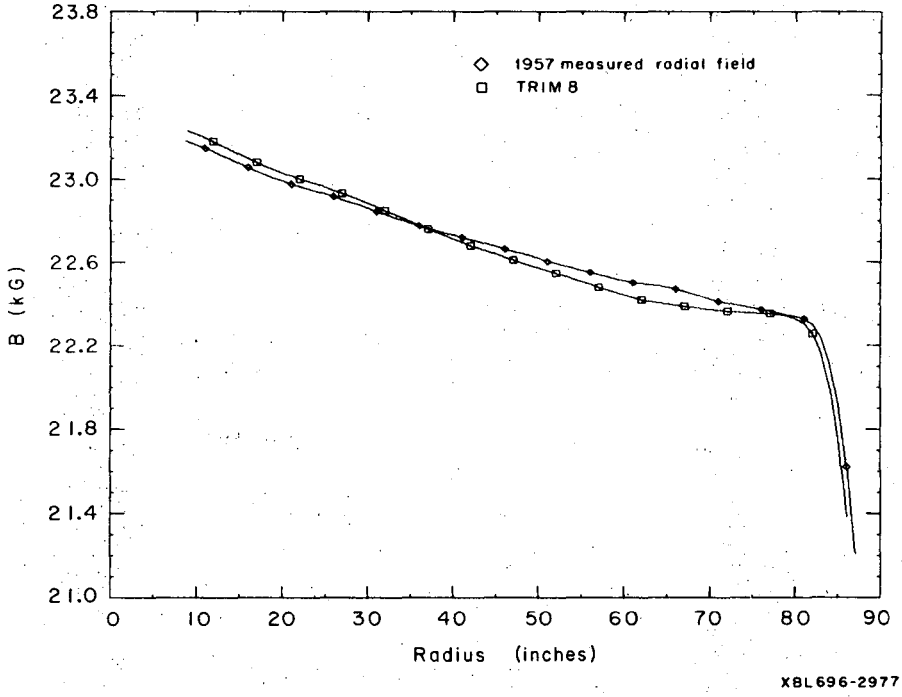

Fig. 6. The measured (standard) magnetic field and computed magnetic field (TRIM-8) at the same excitation as a function of radius.

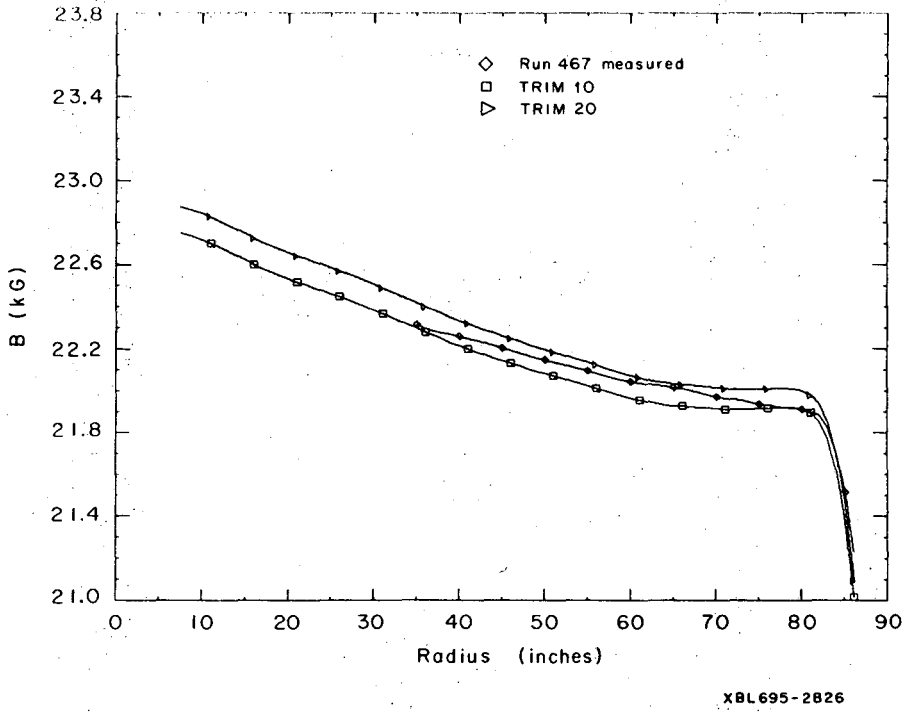

Fig. 7. The measured magnetic field at 162 deg at an auxiliary coil current of 2441 A and the calculated field at the same excitation.

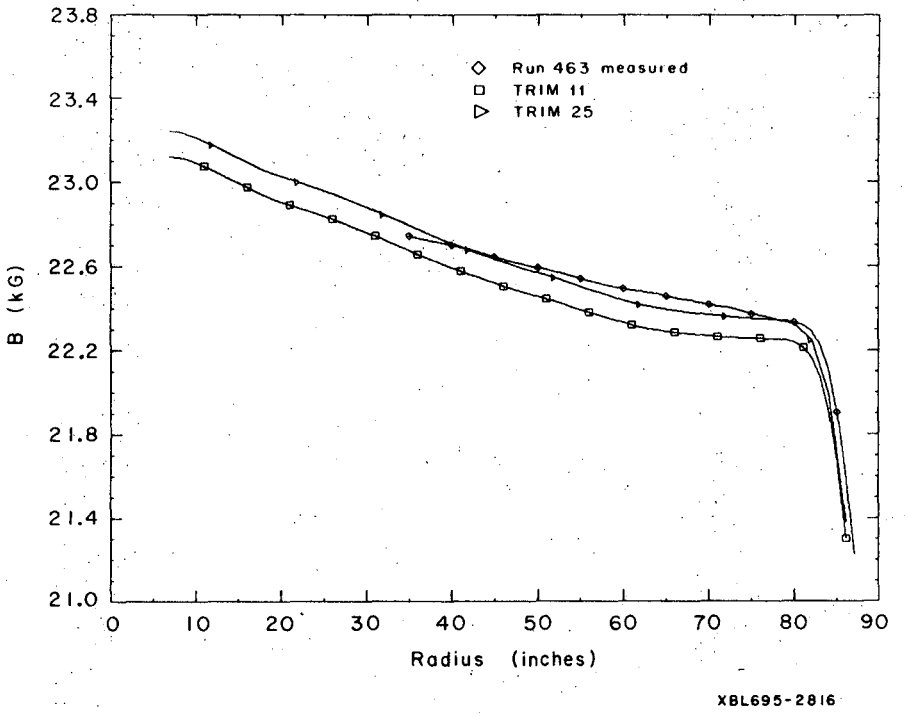

Fig. 8. The measured magnetic field at 162 deg at an auxiliary coil current of 2662 A and the calculated field at the same excitation.

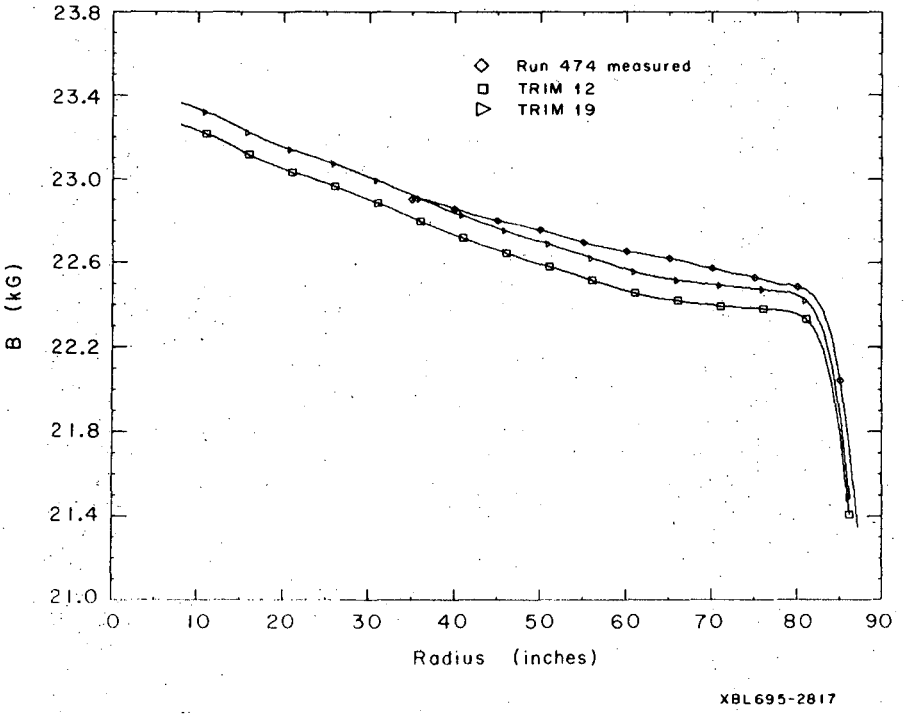

Fig. 9. The measured magnetic field at 162 deg at an auxiliary coil current of 2743 A and the calculated field at the same excitation.

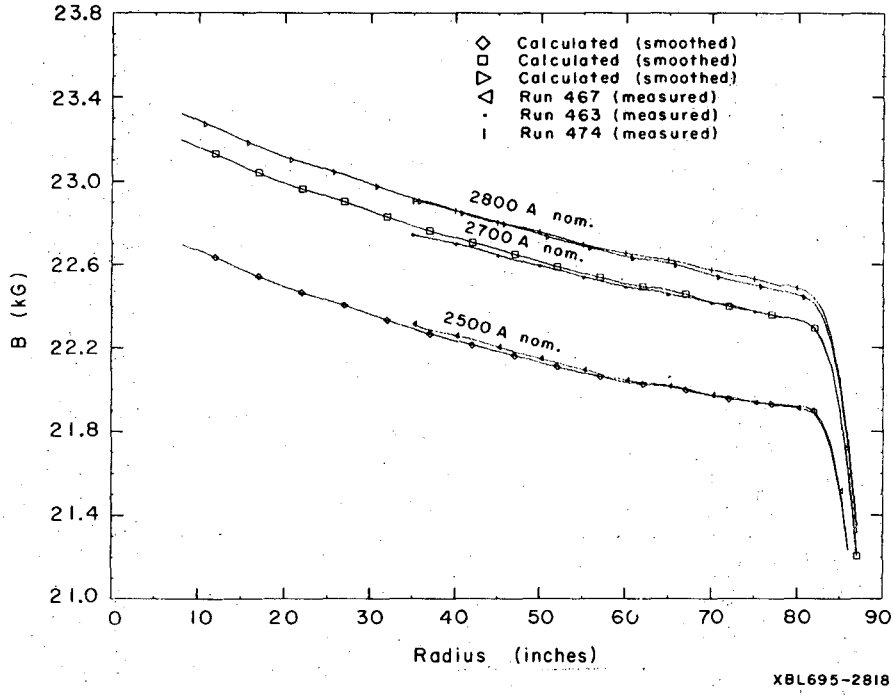

Fig. 10. Measured fields at different excitations and the corresponding calculated fields after corrections for azimuthal averaging and after smoothing by subtraction of the integration errors.

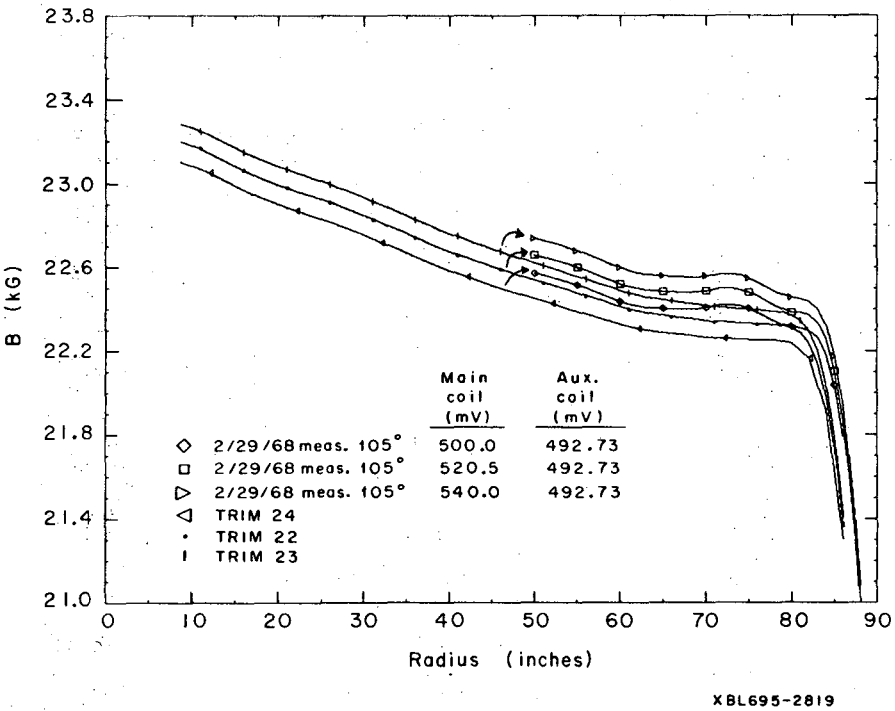

Fig. 11. The measured magnetic field at 105 deg at the present auxiliary coil current of 2678 A and the main coil currents of 1500, 1562, and 1620 A and the corresponding calculated fields at the same excitations.

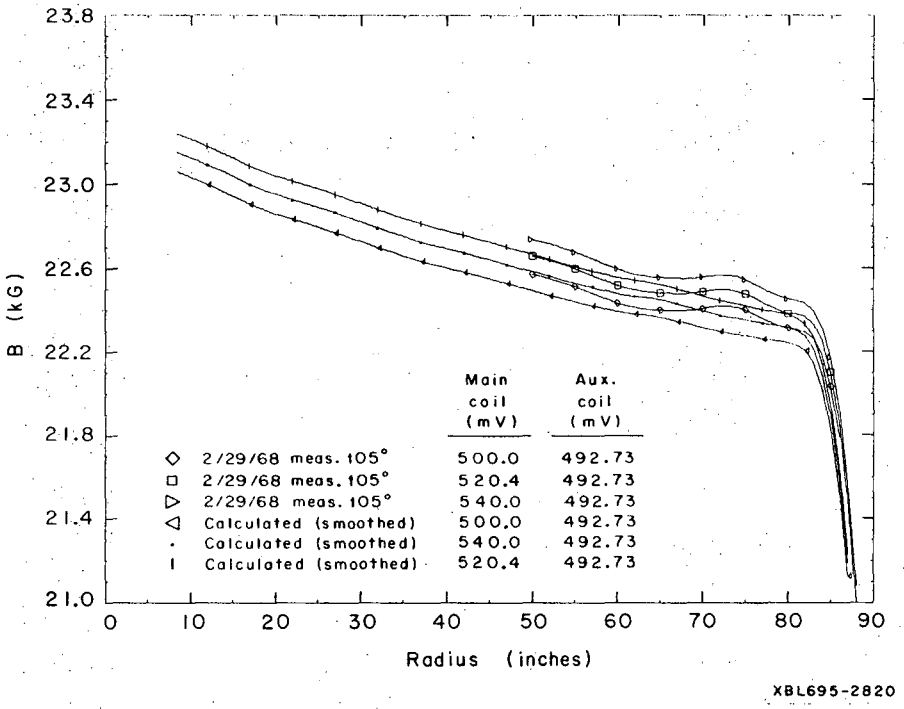

Fig. 12. The measured magnetic fields at 105 deg azimuth at the present auxiliary coil current of 2678 A and main coil currents of 1500, 1562, and 1620 A and the calculated fields at the same excitations after smoothing.

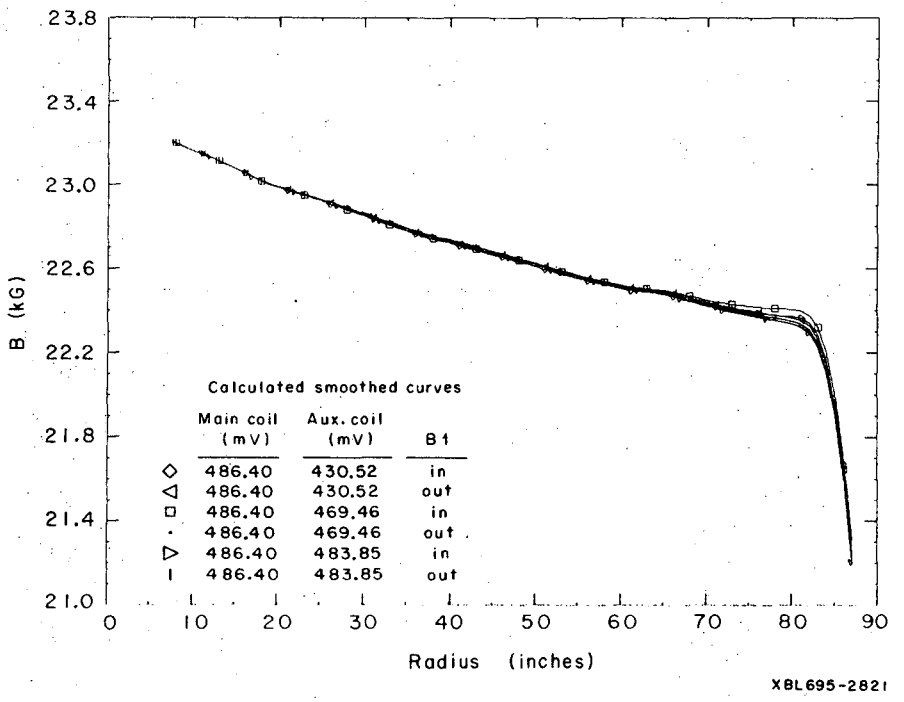

Fig. 13. Smoothed fields at main coil current of 1524 A and auxiliary coil currents at 2441, 2662, and 2743 A normalized to the same value at 15 in. radius.

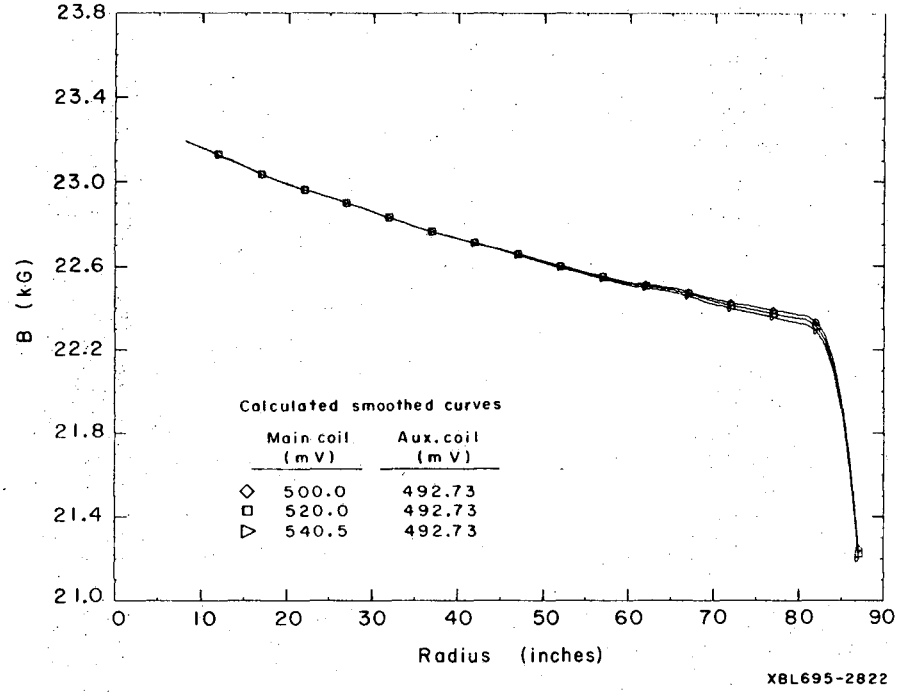

Fig. 14. Smoothed fields at main coil currents of 1500, 1562, and 1620 A and auxiliary coil current of 2675 A normalized to the same values at 15 in. radius.

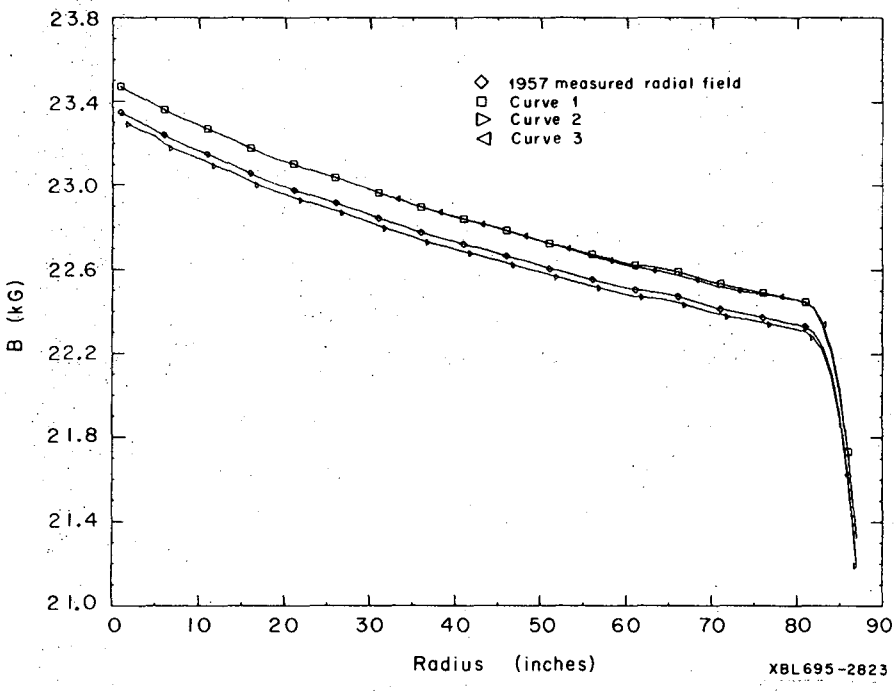

Fig. 15. The standard 1957 measured field. Curve 1 shows the 1957 measured field scaled to the 1968 field at 30 in. radius. Curve 2 shows the smooth calculated field for the present operation currents without stacking factor and universe corrections. Curve 3 shows the 1968 measured field at 105 deg smoothed to remove the regenerator perturbations by subtraction of the 1957 field at 105 deg.

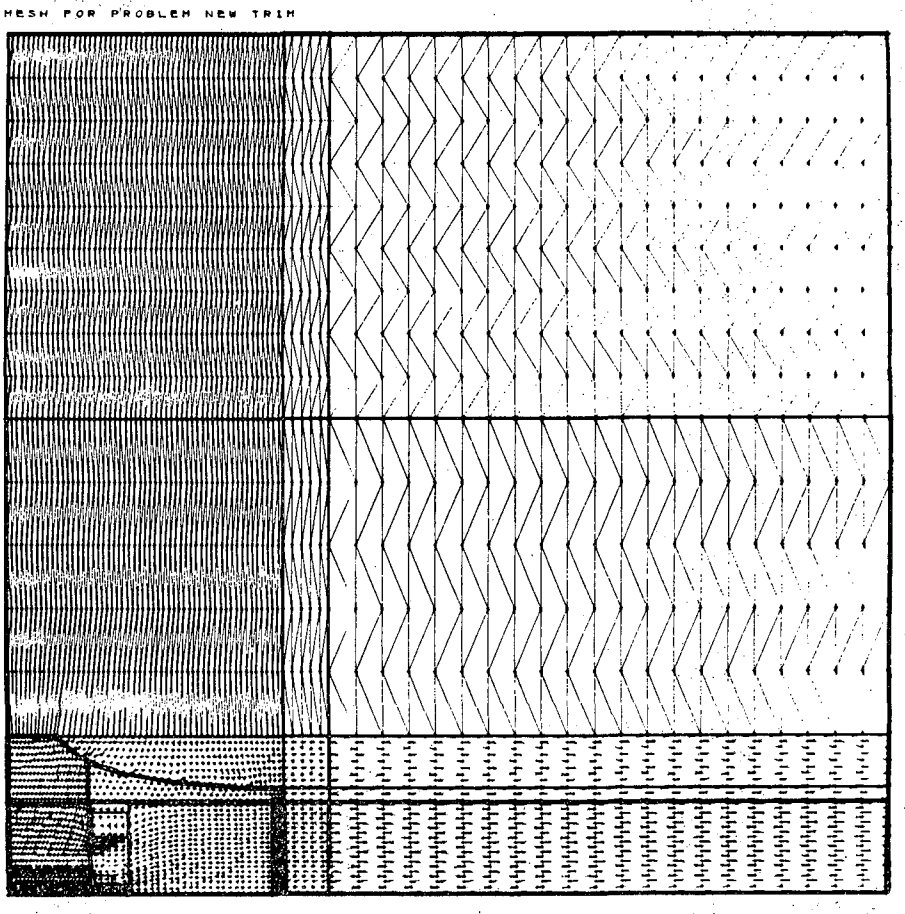

XBL 706-1077

Fig. 16. Modified mesh for extended "universe" of 1000×1000 in.

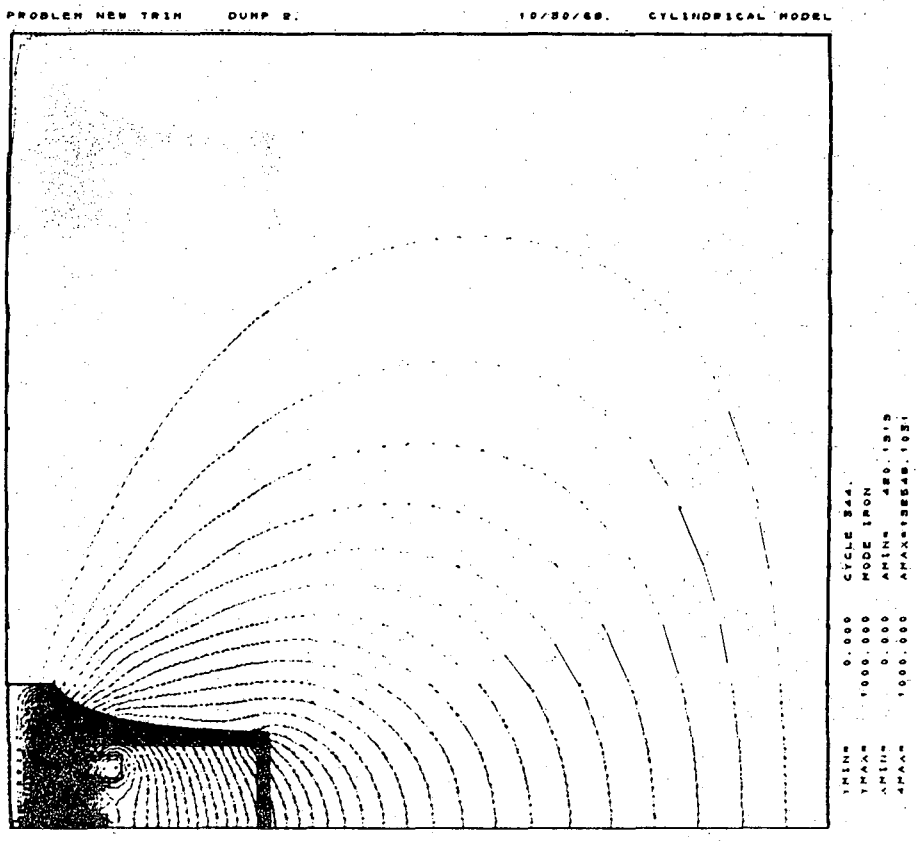

XBL 706-1078

Fig. 17. Flux distribution with extended "universe" of 1000×1000 in.

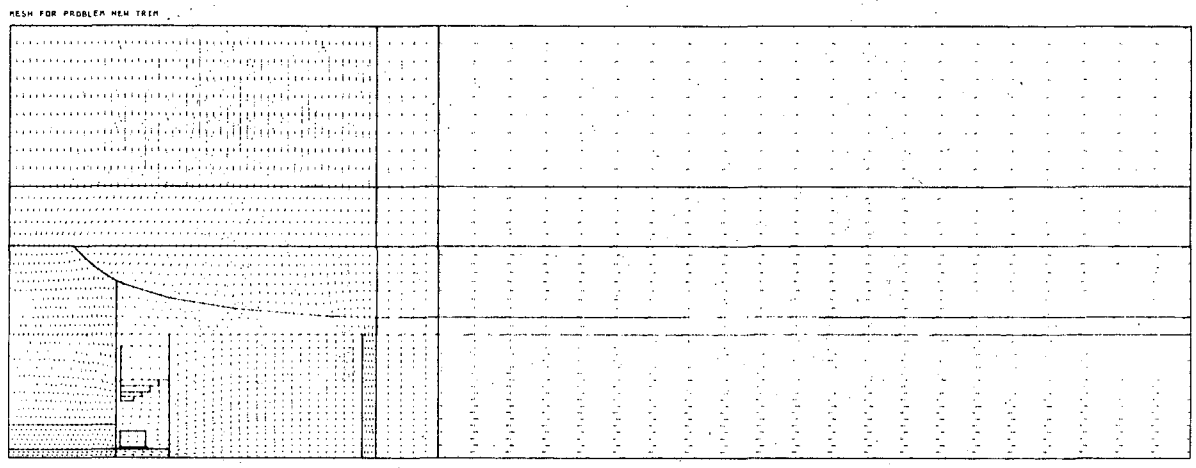

XBL 706-1079

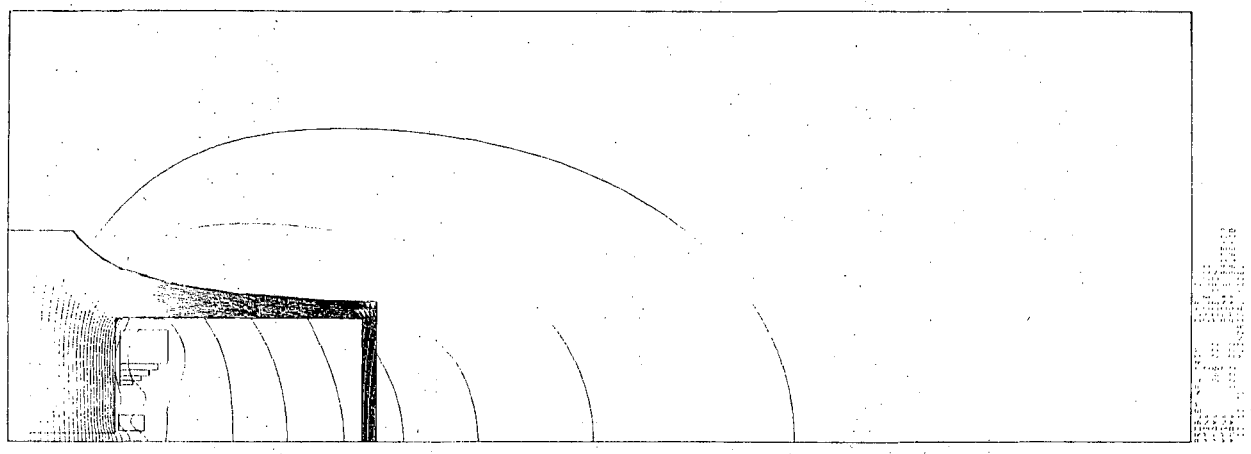

XBL 706-1080

Fig. 18. (a) Mesh with extended "universe" of 365×1000 in.
(b) Flux distribution with extended universe of 365×1000 in.

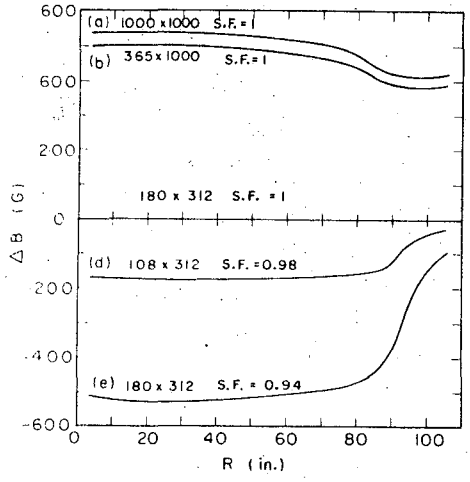

XBL705-2788

Fig. 19. ΔB vs Radius for modified model, showing effect of air boundary and stacking factor.

TECHNICAL INFORMATION DIVISION
LAWRENCE RADIATION LABORATORY
UNIVERSITY OF CALIFORNIA
BERKELEY, CALIFORNIA 94720